Nonlinear resonances of an idealized saccular aneurysm

Abstract

This paper investigates the occurrence of dynamic instabilities in idealized intracranial saccular aneurysms subjected to pulsatile blood flow and surrounded by cerebral spinal fluid. The problem has been approached extending the original 2D model of Shah and Humphrey (1999) to a 3D framework. The justification for using a 3D formulation arises from the works of Suzuki and Ohara (1978), MacDonald et al. (2000) and Costalat et al. (2011) who showed experimental evidences of intracranial aneurysms with a ratio between wall thickness and inner radius larger that 0.1. Two different material models have been used to describe the mechanical behaviour of the aneurysmal wall: Neo-Hookean and Mooney-Rivlin. For the first time in literature the dynamic response of the aneurysm has been analysed using complete nonlinear resonance diagrams that have been obtained from a numerical procedure specifically designed for that purpose. Our numerical results show that, for a wide range of wall thicknesses and both constitutive models considered, the saccular aneurysms are dynamically stable within the range of frequencies associated to the normal heart rates, which confirms previous results of Shah and Humphrey (1999). On the other hand, our results also show that the geometric and material nonlinearities of the problem could bring closer than expected the resonance frequencies of the aneurysm to the frequencies of the pulsatile blood flow.

Keywords:

Intracranial aneurysm, Finite elasticity, Constitutive model, Nonlinear resonances

1. Introduction

The question of whether mechanical instabilities, both static and dynamic, may cause the enlargement and rupture of saccular aneurysms has been debated by the scientific community during the last 40 years. Several researchers, such as Akkas (1990) and Austin et al. (1989), pointed out that the existence of limit point instabilities (i.e. mathematical bifurcations in the quasi-static response of the aneurysm) could be a reason for the growth and rupture of this type of lesions. Alternatively, other authors like Jain (1963), Sekhar and Heros (1981) and Sekhart et al. (1988) suggested that the pulsatile blood flow could excite the natural frequency of the

aneurysm making it dynamically unstable. This hypothesis was supported by the results of Simkins and Stehbens (1973) and Hung and Botwin (1975), who studied the elastodynamics of berry aneurysms and showed that the natural frequency of these type of lesions may lie within the range of bruit frequencies that commonly accompany aneurysms. However, despite the nonlinear stress-strain response exhibited by the aneurysmal wall over finite strains, these authors used in their analysis the classical shell membrane theory, which assumes infinitesimal strains and linear material behaviour. Furthermore, they ignored the contribution of the Cerebral Spinal Fluid (CSF) surrounding the lesion. Thus, the idea that resonances may cause the rupture of intracranial aneurysms has been gradually losing support within the scientific community.

Shah and Humphrey (1999) and David and Humphrey (2003) studied the nonlinear elastodynamics of a sub-class of spherical aneurysms subjected to pulsatile blood pressure and surrounded by CSF. The aneurysmal wall was modelled using a Fung-type pseudostrain-energy function which included strain rate dependence. These works brought to light that both surrounding fluid and material viscosity help to increase the dynamic stability of the aneurysm. Shortly after, Haslach and Humphrey (2004) provided further insights into the effect of the mechanical behaviour of the aneurysmal wall on the dynamic response of the lesion. Through the comparison of various strain energy functions, the authors pointed out the great sensitivity of the dynamic behaviour of the aneurysm to the constitutive model used to describe the aneurysmal wall. In particular, they stressed the fact that it is essential for the (correct) analysis of the dynamic stability of aneurysms to use constitutive models specifically formulated and calibrated for the aneurysmal wall. It was shown that the opposite may give rise to misleading results which predict dynamic instabilities that there are not present in actual tissue.

In this research we revisit the works of Humphrey and co-workers (Shah and Humphrey, 1999; David and Humphrey, 2003; Haslach and Humphrey, 2004) and extend their 2D elastodynamics model to a 3D framework[1] in order to study the dynamic response of idealized saccular aneurysms. While many aneurysmal lesions show small wall thickness and thus can be modelled relying on the membrane hypothesis, the justification for using a 3D formulation arises from the works of Suzuki and Ohara (1978), MacDonald et al. (2000) and Costalat et al. (2011) who obtained experimental evidences of intracranial aneurysms with a ratio between wall thickness and inner radius larger that 0.1, leading to non-negligible radial stresses through the aneurysmal wall. Another

---

[1]For which we have followed the pioneering work of Knowles (1962)

original feature of our research is that the we have obtained, for the first time in literature, the complete nonlinear resonance diagrams that characterize the dynamic response of the aneurysm as a function of the pulsatile blood flow. A Mooney-Rivlin type constitutive model, calibrated by Costalat et al. (2011) using experimental data obtained from 16 different intracranial aneurysms tested under physiological conditions, has been used to describe the mechanical behaviour of the aneurysmal wall. The results are systematically compared with those obtained from a simple Neo-Hookean model widely applied to characterize the behaviour rubber-like materials. This research shows that, for any of the constitutive models used and irrespective of the thickness of the aneurysmal wall, the resonance frequencies of the aneurysm do not lie within the range of frequencies associated to the normal heart rates, which in turn seems to confirm the earlier findings of Shah and Humphrey (1999).

2. Problem formulation

In this section we formulate the problem of an idealized intracranial saccular (spherical) aneurysm surrounded by CSF and subjected to pulsating, and radially symmetric, blood pressure (see Fig. 1). The original contribution is to extend the 2D formulation developed by Humphrey and co-workers (Shah and Humphrey, 1999; David and Humphrey, 2003) to a 3D framework.
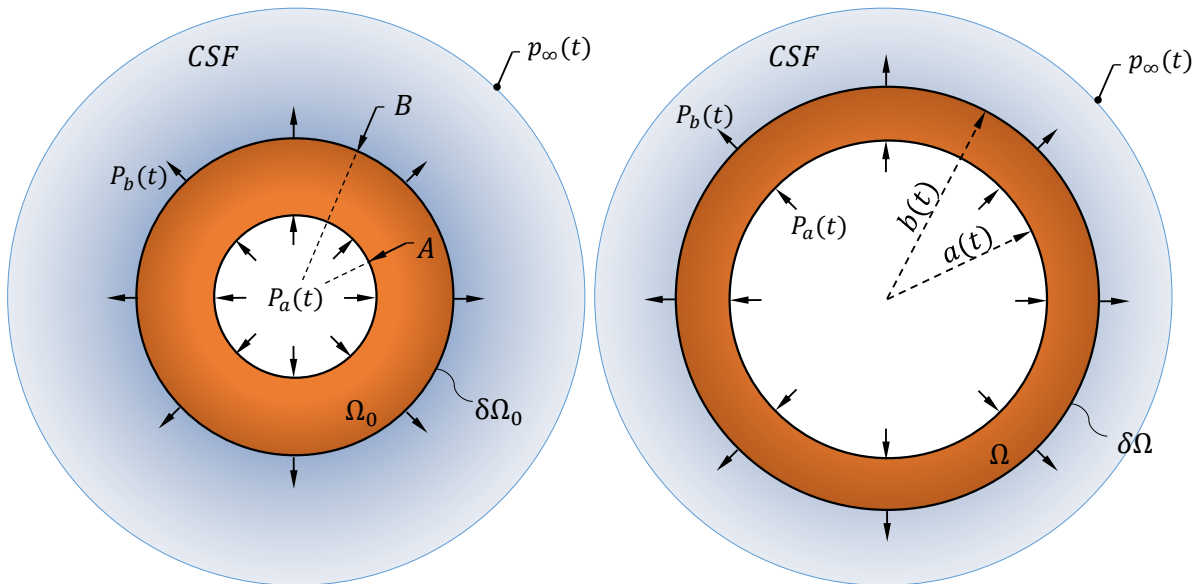

Figure 1: Schematic representation of an idealized saccular (spherical) aneurysm surrounded by cerebral spinal fluid and subjected to radially symmetric pulsating blood pressure. (a) Reference and (b) deformed configurations.

2.1. The aneurysmal wall

Following Shah and Humphrey (1999), the aneurysmal wall is taken to be incompressible and isotropic within the framework of finite nonlinear elasticity. While the hypothesis of homogeneous and isotropic properties is likely a gross approximation (Ryan and Humphrey, 1999), it allow us to follow Humphrey and Haslach (2003) and thus study the elastodynamics of the aneurysmal lesion. The aneurysm occupies a volume Ω_0 defined by the spherical polar coordinates (R, Θ, Φ) in some reference configuration such that $A \leq R \leq B$. In this paper we take $A = 4.3 \ mm$ and $B = 4.67 \ mm$ which, based on the work of Costalat et al. (2011), represent average values for the inner and outer radii of intracranial aneurysmal lesions. Since the material is deformed so that the spherical symmetry is maintained, the motion is given by

$$r = r(R, t); \qquad\qquad \theta = \Theta; \qquad\qquad \phi = \Phi \qquad\qquad (1)$$

where (r, θ, ϕ) are spherical polar coordinates in the current configuration Ω such that $a \leq r \leq b$.

The balance of linear momentum in the radial direction leads to

$$\frac{\partial \sigma_r}{\partial r} + 2\frac{\sigma_r - \sigma_\theta}{r} = \rho \ddot{r} \qquad\qquad (2)$$

where a superposed dot denotes differentiation with respect to time. Moreover $\sigma_r(r, t)$ and $\sigma_\theta(r, t)$ are the radial and circumferential Cauchy stresses respectively and $\rho = 1050 \ kg/m^3$ is the density of the aneurysmal wall (Shah and Humphrey, 1999).

Moreover, let $\lambda_r = \frac{\partial r}{\partial R}$ and $\lambda_\theta = \lambda_\phi = \frac{r}{R} = \lambda$ denote the radial and circumferential stretches respectively. From the incompressibility condition we deduce

$$\lambda(r, t) = \left(\frac{B^3}{R^3}(\lambda_b^3 - 1) + 1\right)^{1/3} \qquad\qquad (3)$$

where $\lambda_b = \frac{b}{B}$ stands for the circumferential stretch in the outer surface of the aneurysmal wall. We take the derivatives of Eq. (3) with respect to r and t to obtain respectively

$$\frac{\partial \lambda}{\partial r} = -\frac{\lambda^3 - 1}{R} \qquad\qquad (4)$$

$$\ddot{\lambda} = \frac{\lambda^3 - 1}{\lambda_b^3 - 1}\left(\frac{2\lambda_b\dot{\lambda_b}^2 + \lambda_b^2\ddot{\lambda_b}}{\lambda^2} - \frac{2\,\lambda_b^4\dot{\lambda_b}^2}{\lambda_b^3 - 1}\frac{\lambda^3 - 1}{\lambda^5}\right) \qquad\qquad (5)$$

Previous expressions are inserted into Eq. (2) to obtain

$$\frac{\partial \sigma_r}{\partial \lambda} - 2\frac{\sigma_r - \sigma_\theta}{\lambda(\lambda^3-1)} = -\rho B^2 \frac{2\lambda_b \dot{\lambda_b}^2 + \lambda_b^2 \ddot{\lambda_b}}{(\lambda_b^3-1)^{1/3}}\frac{1}{\lambda^2(\lambda^3-1)^{2/3}} + \rho B^2 \frac{2\,\lambda_b^4 \dot{\lambda_b}^2}{(\lambda_b^3-1)^{4/3}}\frac{(\lambda^3-1)^{1/3}}{\lambda^5} \quad (6)$$

Moreover, for an incompressible spherical shell we have that (see e.g. Ogden (1997))

$$\sigma_r - \sigma_\theta = -\frac{1}{2}\lambda\frac{d\psi}{d\lambda}(\lambda^{-2}, \lambda, \lambda) \quad (7)$$

where ψ is the strain energy function which determines the mechanical behaviour of the material. The specific form of ψ will be defined in section 3.

With help of Eq. (7), we integrate Eq. (6) over the thickness of the aneurysm to obtain

$$P_a(t) - P_b(t) = \int_{\lambda_b}^{\left(\frac{\lambda_b^3 + f_0 - 1}{f_0}\right)^{1/3}} \frac{\psi'}{\lambda^3 - 1}\,d\lambda - \rho B^2\left(1 - \frac{\lambda_b}{(\lambda_b^3+f_0-1)^{1/3}}\right)\lambda_b\ddot{\lambda_b} - \rho B^2\left(\frac{3}{2} + \frac{\lambda_b^4}{2(\lambda_b^3+f_0-1)^{4/3}} - \frac{2\lambda_b}{(\lambda_b^3+f_0-1)^{1/3}}\right)\dot{\lambda_b}^2 \quad (8)$$

where the superscript prime denotes differentiation with respect to the circumferential stretch. Moreover, $f_0 = \frac{A^3}{B^3} = 0.78$ is a dimensionless parameter which characterizes the thickness of the aneurysmal wall. $P_a(t)$ and $P_b(t)$ are the blood pressure and the pressure exerted by the CSF on the aneurysm, respectively. The specific forms of $P_a(t)$ and $P_b(t)$ are provided in sections 2.2 and 2.3.

2.2. Blood pressure

Based on the data measured by Ferguson (1972) for human saccular aneurysms, and assuming that the pressure is uniform inside the lesion, the blood pressure is represented by the following Fourier series

$$P_a(t) = P_m + \sum_{n=1}^{N}(A_n\cos(n\omega t) + B_n\sin(n\omega t)) \quad (9)$$

where $P_m = 67.5\,mmHg$ is the mean pressure (Shah and Humphrey, 1999), A_n and B_n are the fourier coefficients for N harmonics, and ω is the fundamental circular frequency. Following Shah and Humphrey (1999) we have considered 5 harmonics: $A_1 = -7.13$, $B_1 = 4.64$, $A_2 = -3.08$, $B_2 = -1.18$, $A_3 = -0.130$, $B_3 = -0.564$, $A_4 = -0.205$, $B_4 = -0.346$, $A_5 = 0.0662$ and $B_5 = -0.120$, all quantities are given in $mmHg$.

2.3. Cerebral spinal fluid

The CSF is assumed incompressible and Newtonian. The continuity equation takes the form

$$\frac{1}{r^2}\frac{\partial}{\partial r}(r^2\,v_r) = 0 \tag{10}$$

Previous expression implies that the radial velocity is $v_r(r,t) = \frac{c(t)}{r^2}$. The function $c(t)$ is found matching the fluid and aneurysmal wall velocities at $r = b$. Thus, we obtain the following expression that relates the radial velocity of the CSF and the stretch (and stretch rate) in the outer surface of the aneurysm

$$v_r(r,t) = \frac{B^3\lambda_b^2\dot{\lambda}_b}{r^2} \tag{11}$$

Moreover, the balance of linear momentum along the radial direction takes the form

$$\rho_f\left(\frac{\partial v_r}{\partial t} + v_r\frac{\partial v_r}{\partial r}\right) = -\frac{\partial p}{\partial r} + \mu\left(\frac{1}{r^2}\frac{\partial}{\partial r}\left(r^2\frac{\partial v_r}{\partial r}\right) - 2\frac{v_r}{r^2}\right) \tag{12}$$

where p denotes pressure. Moreover, $\rho_f = 1000\ kg/m^3$ and $\mu = 1.2610^{-4}\ Ns/m^2$ are the density and the viscosity of the CSF, respectively (Shah and Humphrey, 1999).

Next, we insert Eq. (11) into Eq. (12) to obtain

$$\frac{\partial p}{\partial r} = -\rho_f\left(\frac{B^3}{r^2}\left(\lambda_b^2\ddot{\lambda}_b + 2\lambda_b\dot{\lambda}_b^2\right) - \frac{2B^6\lambda_b^4}{r^5}\dot{\lambda}_b^2\right) \tag{13}$$

Integrating previous equation over the range $r \in (b,\infty)$, we obtain an expression for the static pressure exerted by the CSF on the outer surface of the aneurysm

$$p_b^s(t) = p_\infty + \rho_f B^2\left(\lambda_b\ddot{\lambda}_b + \frac{3}{2}\dot{\lambda}_b^2\right) \tag{14}$$

where $p_\infty = 3\ mmHg$ is the remote pressure assumed constant (Shah and Humphrey, 1999).

Next, relying on the constitutive equations of incompressible Newtonian fluids, we compute the dynamic pressure (radial stress) caused by the deformation of the CSF on the aneurysmal wall

$$p_b^d(t) = 4\mu\frac{\dot{\lambda}_b}{\lambda_b} \tag{15}$$

Thus, the total pressure exerted by the cerebral spinal fluid on the outer surface of the aneurysm is

$$P_b(t) = -p_b^s(t) - p_b^d(t) \tag{16}$$

2.4. Dimensionless governing equation

We introduce the following length, mass and time scales in order to pose the problem in non-dimensional form

$$[L] = B; \qquad [M] = \rho B^3; \qquad [T] = \sqrt{\frac{\rho B^2}{C_{M10}}} \tag{17}$$

where C_{M10} is a material constant as further discussed in section 3.

Previous non-dimensional groups, together with Eqs. (9) and (16), are inserted into Eq. (8) to obtain the following dimensionless governing equation which shows that λ_b is the only unknown of the problem

$$\overline{\Delta P} = \int_{\lambda_b}^{\left(\frac{\lambda_b^3 + f_0 - 1}{f_0}\right)^{1/3}} \frac{\overline{\psi}'}{\lambda^3 - 1} d\lambda + 4\kappa \frac{\dot{\lambda}_b}{\lambda_b} + \overline{\rho}\left(\lambda_b \ddot{\lambda}_b + \frac{3}{2}\dot{\lambda}_b^2\right)$$
$$- \left(\left(1 - \frac{\lambda_b}{(\lambda_b^3 + f_0 - 1)^{1/3}}\right)\lambda_b \ddot{\lambda}_b + \left(\frac{3}{2} + \frac{\lambda_b^4}{2(\lambda_b^3 + f_0 - 1)^{4/3}} - \frac{2\lambda_b}{(\lambda_b^3 + f_0 - 1)^{1/3}}\right)\dot{\lambda}_b^{\,2}\right) \tag{18}$$

where

$$\overline{\Delta P} = \overline{P}_m + \sum_{n=1}^{N}\left(\overline{A}_n \cos(n\tau\overline{\omega}) + \overline{B}_n \sin(n\tau\overline{\omega})\right) - \overline{p}_\infty \tag{19}$$

Now a superposed dot denotes differentiation with respect to the dimensionless time τ. Note that when $f_0 \to 1$ we recover Eq. (12) of Shah and Humphrey (1999). The adimensionalization procedure brings to light 8 additional non-dimensional groups (additional to f_0 introduced in Eq. (8)) that govern the problem at hand

$$\overline{\psi} = \frac{\psi}{C_{M10}} \qquad \overline{P}_m = \frac{P_m}{C_{M10}} \qquad \overline{p}_\infty = \frac{p_\infty}{C_{M10}}$$

$$\overline{A}_i = \frac{A_i}{C_{M10}} \qquad \overline{B}_i = \frac{B_i}{C_{M10}} \quad \text{for} \quad i = 1, 2, 3, 4, 5$$

$$\overline{\omega} = \omega\sqrt{\frac{\rho B^2}{C_{M10}}} \qquad \kappa = \frac{\mu}{B\sqrt{\rho\, C_{M10}}} \qquad \overline{\rho} = \frac{\rho_f}{\rho}$$

where $\overline{\psi}$ is the non-dimensional strain energy function, $\overline{P}_m$ is the dimensionless mean pressure applied in the inner surface of the aneurysm, $\overline{p}_\infty$ is the dimensionless remote pressure and $\overline{A}_i$ and $\overline{B}_i$ are the dimensionless harmonics coefficients. Moreover, $\overline{\omega}$ is the dimensionless fundamental frequency, κ defines the ratio between the characteristic time scales of CSF and aneurysmal wall and $\overline{\rho}$ is the ratio between CSF and aneurysmal wall densities. Note that in section 5 we will systematically vary $\overline{\omega}$ in order to obtain the resonance diagrams of the aneurysm.

3. Constitutive modelling

Two different strain energy functions are used to describe the mechanical behaviour of the aneurysmal wall. They both respond to the following polynomial form

$$\psi = \sum_{i,j=0}^{N} C_{ij}(I_1 - 3)^i (I_2 - 3)^j \tag{20}$$

where C_{ij} are empirically determined material parameters and I_1, I_2 are the first and second invariants of the left Cauchy-Green strain tensor, respectively. Namely, we use the so-called Neo-Hookean and 3-parameters Mooney-Rivlin models.

- Neo-Hookean model

$$\psi = C_{\mathrm{N10}}(I_1 - 3) \tag{21}$$

- 3-parameters Mooney-Rivlin model

$$\psi = C_{\mathrm{M10}}(I_1 - 3) + C_{\mathrm{M01}}(I_2 - 3) + C_{\mathrm{M11}}(I_1 - 3)(I_2 - 3) \tag{22}$$

The 3-parameter Mooney-Rivlin model was calibrated by Costalat et al. (2011) using experimental results obtained from 16 intracranial saccular aneurysms tested in uniaxial tension under physiological conditions. The resulting parameters values are: $C_{\mathrm{M10}} = 0.19 \ MPa$, $C_{\mathrm{M01}} = 0.024 \ MPa$ and $C_{\mathrm{M11}} = 7.87 \ MPa$. For the Neo-Hookean model we have taken $C_{\mathrm{N10}} = 0.214 \ MPa$, which ensures that Neo-Hookean and Mooney-Rivlin models provide the same shear modulus in the linear limit. While both constitutive models were originally formulated for rubber-like materials, they have been widely used in the literature to model the mechanical behaviour of aneurysms (Tóth et al., 2005; Gundiah et al., 2007; Costalat et al., 2011). The comparison

between Neo-Hookean and Mooney-Rivlin models developed in section 5 brings to light the key role played by the mechanical behaviour of the aneurysmal wall in the dynamic response of the aneurysm.

4. Numerical solution

In this section we describe the numerical procedure designed to analyse the dynamic response of the aneurysm. The numerical scheme relies on two main techniques: a *shooting method* and a *sequential continuation method*. The combination of these two techniques allows to obtain the resonance diagrams of the aneurysmal lesion presented in section 5.

Firstly, we reduce Eq. (18) to the following system of two first-order differential equations where $x_1 = \lambda_b$ and $x_2 = \dot{\lambda}_b$

$$\dot{x}_1 = x_2 \tag{23}$$

$$\dot{x}_2 = \frac{\overline{\Delta P} - \int_{x_1}^{\left(\frac{x_1^3 + f_0 - 1}{f_0}\right)^{1/3}} \frac{\overline{\psi}'(\lambda)}{\lambda^3 - 1} \, d\lambda - 4\kappa \frac{x_2}{x_1} + \left(\frac{3}{2} + \frac{x_1^4}{2(x_1^3 + f_0 - 1)^{4/3}} - \frac{2x_1}{(x_1^3 + f_0 - 1)^{1/3}} - \frac{3}{2}\overline{\rho}\right) x_2^2}{\left(\overline{\rho} + \frac{x_1}{(x_1^3 + f_o - 1)^{1/3}} - 1\right) x_1} \tag{24}$$

The harmonically forced system described by Eqs. (23)-(24) is transformed into an autonomous system adding the following two differential equations whose stable solutions are the non-autonomous terms

$$\dot{x}_3 = x_3(1 - x_3^2 - x_4^2) - \overline{w}x_4 \tag{25}$$

$$\dot{x}_4 = x_4(1 - x_3^2 - x_4^2) + \overline{w}x_3 \tag{26}$$

Taking as initial conditions $x_3(0) = 1$ and $x_4(0) = 0$, the solutions of these equations are $x_3(\tau) = \sin(\overline{w}\tau)$ and $x_4(\tau) = \cos(\overline{w}\tau)$, respectively. Expanding[2] Eq. (9) in terms of $\sin(\overline{w}\tau)$ and $\cos(\overline{w}\tau)$, the problem can be handled as an autonomous system of dimension $n = 4$ that has the following vectorial form

---

[2]The trigonometric expansion is given by $\sin(n\alpha) = \sum_{k=0}^{n} \binom{n}{k} \cos^k \alpha \, \sin^{n-k} \alpha \, \sin(1/2(n-k)\pi)$ and $\cos(n\alpha) = \sum_{k=0}^{n} \binom{n}{k} \cos^k \alpha \, \sin^{n-k} \alpha \, \cos(1/2(n-k)\pi)$

$$\frac{d\mathbf{x}}{d\tau} = \mathbf{F}(\mathbf{x}) \tag{27}$$

where $\mathbf{x} = (x_1, x_2, x_3, x_4)$.

We limit our attention to the periodic response of the aneurysm (resonances) and thus the solutions of interest satisfy the condition $\mathbf{x}(\tau) = \mathbf{x}(\tau + \Gamma)$ where Γ is the period of the oscillation. This allows to formulate the following two-point boundary value problem

$$\frac{d\mathbf{x}}{d\tau} = \mathbf{F}(\mathbf{x}); \quad \mathbf{x}(0) = \mathbf{x}_0; \quad \mathbf{x}(\Gamma) = \mathbf{x}_0 \tag{28}$$

where $\mathbf{x}_0$ is the initial conditions vector. Note that $\mathbf{x}_0$ and Γ are, *a priori*, unknown.

4.1. Shooting method

The problem defined by (28) is solved using the *shooting method* (Seydel, 1994; Allgower and Kurt, 1990; Peeters et al., 2009). For that purpose, we define the periodicity condition

$$\mathbf{H}(\mathbf{x}_0, \Gamma) \equiv \mathbf{x}(\mathbf{x}_0, \Gamma) - \mathbf{x}_0 = 0 \tag{29}$$

where $\mathbf{H}(\mathbf{x}_0, \Gamma)$ is the so called *shooting function*. Note that the solution at time Γ is now expressed as $\mathbf{x}(\mathbf{x}_0, \Gamma)$ in order to highlight the dependence of the problem solution with the initial conditions $\mathbf{x}_0$.

The shooting technique starts with a trial value for $(\mathbf{x}_0, \Gamma)$. The solution of the system then is obtained by numerical integration of the system of equations (23)-(26). In general, the trial value will not satisfy the periodicity condition given by Eq. (29). Therefore, a Newton-Raphson iteration scheme is used to correct the initial trial and converge to the actual solution. The corrections $(\Delta \mathbf{x}_0, \Delta \Gamma)$ are obtained from the following linear expansion of the periodicity condition

$$\mathbf{H}(\mathbf{x}_0 + \Delta \mathbf{x}_0, \Gamma + \Delta \Gamma) \approx \mathbf{H}(\mathbf{x}_0, \Gamma) + \left.\frac{\partial \mathbf{H}}{\partial \mathbf{x}_0}\right|_{(\mathbf{x}_0, \Gamma)} \Delta \mathbf{x}_0 + \left.\frac{\partial \mathbf{H}}{\partial \Gamma}\right|_{(\mathbf{x}_0, \Gamma)} \Delta \Gamma + \text{H.O.T} = 0 \tag{30}$$

where the coefficients of previous linear system $(\partial \mathbf{H}/\partial \Gamma, \partial \mathbf{H}/\partial \mathbf{x}_0)$ are to be calculated.

From Eq. (29) it follows that the $2n \times 1$ coefficient vector $\partial \mathbf{H}/\partial \Gamma$ is

$$\frac{\partial \mathbf{H}}{\partial \Gamma}(\mathbf{x}_0, \Gamma) = \left.\frac{\partial \mathbf{x}(\tau, \mathbf{x}_0)}{\partial \tau}\right|_{\Gamma} = \mathbf{F}(\mathbf{x}_0) \tag{31}$$

Also from Eq. (29) it follows that the $2n \times 2n$ Jacobian matrix $\partial \mathbf{H}/\partial \mathbf{x}_0$ is

$$\frac{\partial \mathbf{H}}{\partial \mathbf{x}_0}(\mathbf{x}_0, \Gamma) = \left.\frac{\partial \mathbf{x}(\tau, \mathbf{x}_0)}{\partial \mathbf{x}_0}\right|_{\Gamma} - \mathbf{I} \tag{32}$$

where $\mathbf{I}$ is the $2n \times 2n$ identity matrix. The matrix $\partial \mathbf{x}(\tau, \mathbf{x}_0)/\partial \mathbf{x}_0$ is calculated as described by Peeters et al. (2009). For that task, we differentiate the system of equations (23)-(26) with respect to the initial conditions

$$\frac{\partial}{\partial \mathbf{x}_0}\left(\frac{\mathrm{d}\mathbf{x}(\tau, \mathbf{x}_0)}{\mathrm{d}\tau}\right) = \frac{\partial \mathbf{F}(\mathbf{x}(\tau, \mathbf{x}_0))}{\partial \mathbf{x}_0} \tag{33}$$

We change the order of the derivatives in the left hand side of previous equation and apply the chain rule in the right hand side to obtain

$$\frac{\mathrm{d}}{\mathrm{d}\tau}\left(\frac{\partial \mathbf{x}(\tau, \mathbf{x}_0)}{\partial \mathbf{x}_0}\right) = \frac{\partial \mathbf{F}(\mathbf{x})}{\partial \mathbf{x}}\frac{\partial \mathbf{x}(\tau, \mathbf{x}_0)}{\partial \mathbf{x}_0} \tag{34}$$

with initial conditions $\partial \mathbf{x}(0, \mathbf{x}_0)/\partial \mathbf{x}_0 = \mathbf{I}$. The matrix $\partial \mathbf{x}(\tau, \mathbf{x}_0)/\partial \mathbf{x}_0$ for $\tau = \Gamma$ can be thus calculated integrating numerically previous expression.

In order to determine the $2n + 1$ corrections $(\Delta \mathbf{x}_0, \Delta \Gamma)$ we need an additional equation to be added to the system of $2n$ equations defined by (30). The additional equation is obtained following Seydel (1994). For an autonomous system the periodic solutions are invariant to linear shifts of the time origin, which implies that the phase of the solution is arbitrary. Thus, a restriction (so called *phase condition*) must be imposed to remove this arbitrariness. For this task, we set one component of the initial values vector $\mathbf{x}_0$ equal to zero. In the problem at hand, it is especially suited to take $x_2 = 0$ since this amounts to consider that the stretch rate of the outer surface of the aneurysm is initially zero (system initially at rest).

We carry out this iteration process to obtain $\mathbf{x}(\mathbf{x}_0, \Gamma)$ until the following convergence condition, taken from Peeters et al. (2009) and Sracic and Allen (2011), is reached

$$\frac{||\mathbf{H}(\mathbf{x}_0, \Gamma)||}{||\mathbf{x}_0||} < \varepsilon \tag{35}$$

where $\varepsilon = 10^{-6}$ is the tolerance.

4.2. Sequential continuation

Once we have found a solution $\mathbf{x}^j(\mathbf{x}_0^j, \Gamma^j)$ for the normalized frequency $\overline{\omega}^j$, this input parameter is incremented by $\Delta\overline{\omega}^j$

$$\overline{\omega}^{j+1} = \overline{\omega}^j + \Delta\overline{\omega}^j \tag{36}$$

The shooting method then restarts to calculate the corresponding solution $\mathbf{x}^{j+1}(\mathbf{x}_0^{j+1}, \Gamma^{j+1})$ using the current solution $(\mathbf{x}_0^j, \Gamma^j)$ as the initial trial. The sequential continuation method highlights due to its robustness and relatively small computational cost. Nevertheless, we acknowledge that it fails at the bifurcation points of the resonance diagrams, as further discussed in section 5.

4.3. Stability of the periodic solution

The stability of the solution corresponding to each value of $\overline{\omega}$ considered is evaluated using Floquet theory. For that purpose we monitor the eigenvalues of the so called *Monodromy matrix* $\frac{\partial \mathbf{x}(\Gamma, \mathbf{x}_0)}{\partial \mathbf{x}_0}$ (that appeared in (34)). If the modulus of any eigenvalue is greater than 1 the periodic solution is unstable. The classical unit circle representation (Fig. 2) shows that the loss of stability can take place in three different ways:

i. A real eigenvalue exits the unit circle at $(1, 0)$. This represents a transcritical, cyclic-fold or symmetry-breaking bifurcation.

ii. A real eigenvalue exits the unit circle at $(-1, 0)$. This represents a period doubling bifurcation.

iii. A complex conjugate pair of eigenvalues exit the unit circle anywhere else. This represents a secondary Hopf or Niemark bifurcation.

The stability of the solution is further discussed in section 5 when the numerical results are presented.

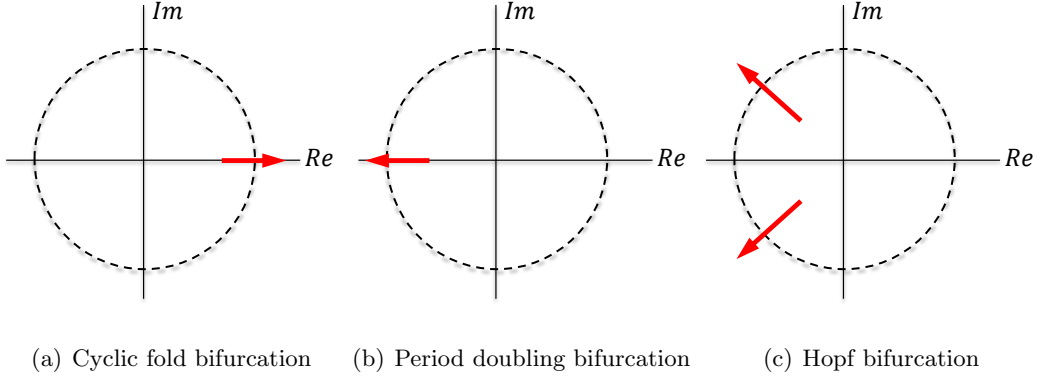(a) Cyclic fold bifurcation   (b) Period doubling bifurcation   (c) Hopf bifurcation

Figure 2: Unit circle representation: imaginary versus real part of the eigenvalues of the Monodromy matrix. Three different scenarios which lead to the loss of stability of the solution: (a) cyclic-fold bifurcation, (b) period doubling bifurcation and (c) Hopf bifurcation.

5. Sample results

The goal of this section is to provide sample numerical results which bring to light the relation between the applied frequency $\bar{\omega}$ and the amplitude of the periodic motion of the aneurysm. In order to carry out this analysis, we first need to characterize (for each frequency) the transient response of the system: the end of the transient regime determines the onset of the periodic motion.

Fig. 3 shows: (a) the pressure applied on the aneurysm $\overline{\Delta P}$ versus the loading time τ, (b) the circumferential stretch in the outer surface of the aneurysm λ_b versus the loading time τ and (c) the circumferential stretch rate $\dot{\lambda}_b$ versus the circumferential stretch λ_b in the outer surface of the aneurysm (phase diagram). While Fig. 3(a) is obtained directly from Eq. (9), Figs. 3(b) and (c) have been obtained after solving equations (23) and (24) using a fourth order Runge-Kutta method. We have taken $\bar{\omega} = 1$ and assumed that the aneurysm is initially unstretched and at rest. The Mooney-Rivlin constitutive model is considered. The geometric, loading and material parameters used in the calculation are those reported in sections 2 and 3, with a single exception: the viscosity of the fluid has been increased to obtain $\kappa = 0.1$. The purpose is to provide a clear illustration of the dissipation of energy by the CSF.

Fig. 3(a) shows the dependence of the applied pressure with time, where Γ is the period given by $\bar{\omega}$ and determined by the time elapsed between two consecutive peaks. Fig. 3(b) enables to identify the transient and steady-state regimes in the oscillatory response of the system. The transient regime lasts until $\tau \approx 30$ and it is characterized by the gradual decrease in the

amplitude of the oscillations of the aneurysm (dashed line). This behaviour is caused by the energy dissipated by the CSF. The steady-state regime, which develops for $\tau \gtrsim 30$, is characterized by the periodic response of the aneurysm (solid line). One can identify a repetitive pattern in the $\lambda_b - \tau$ curve which is determined by the period Γ previously noted in Fig. 3(a). Fig. 3(c) shows the phase diagram corresponding to the outer surface of the aneurysm. We observe that the transient response (dashed line) is also characterized by a gradual decrease in the velocity of the oscillations of the aneurysm. The oscillations become slower and shorter in amplitude until the motion becomes periodic, as illustrated by the limit cycle identified by a solid line. Note that the limit cycle is non-symmetric, which implies the existence of symmetry breaking bifurcations. This limit cycle (characterized by the period Γ), which results from the balance between the work of the applied pressure and the energy dissipated by the CSF, is the focus of our attention in the forthcoming analysis. Namely, our aim is to identify the dependences of the amplitude of the limit cycle with the applied frequency, the thickness of the aneurysm and the specific constitutive model used to describe the aneurysmal wall.
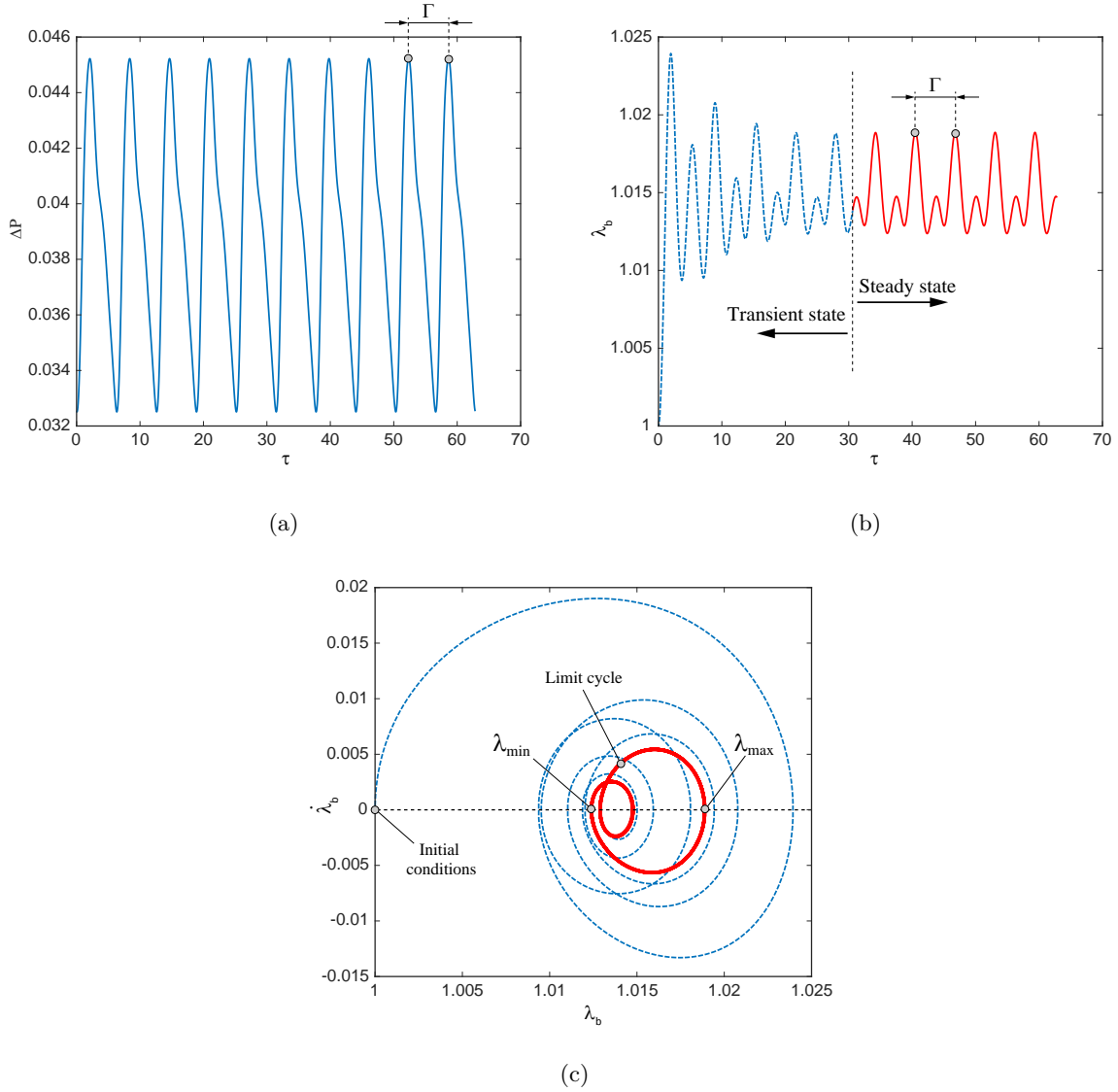
Figure 3: (a) Pressure applied in the inner surface of the aneurysm $\overline{\Delta P}$ versus loading time τ, (b) circumferential stretch in the outer surface of the aneurysm λ_b versus loading time τ and (c) circumferential stretch rate $\dot{\lambda}_b$ versus circumferential stretch λ_b in the outer surface of the aneurysm (phase diagram). The Mooney-Rivlin constitutive model is considered. The normalized frequency is $\bar{\omega} = 1$. The aneurysm is initially unstretched and at rest.

Fig. 4(a)-(b) show the resonance diagrams, $\lambda_{max} - \lambda_{min}$ versus $\bar{\omega}$, for Neo-Hookean and Mooney-Rivlin constitutive models, respectively. Note that λ_{max} and λ_{min} are the maximum and minimum stretches of the limit cycle, as indicated in Fig. 3(c). The geometric, loading and material parameters reported in sections 2 and 3 are used in the calculations, including the fluid viscosity (unlike in previous example). The normalized frequencies investigated range from 0.01 to 100.

The excursions in $\lambda_{max} - \lambda_{min}$ correspond to resonances of the aneurysm: dramatic increase of the amplitude of the oscillations for some specific frequencies. Note that these excursions are tilted, which illustrates the interplay between the natural frequency and the amplitude of the oscillations. This interplay is caused by the nonlinear nature of the problem at hand, which includes geometric and material nonlinearities. The excursion which leads to the maximum amplitude of the oscillations is the so-called fundamental (or primary) resonance of the aneurysm. The other excursions are the so-called super-harmonic resonances. We have calculated the stable and unstable branches of the excursions, which are plotted using solid and dashed lines in Fig. 4(a)-(b), respectively. While the sequential continuation method fails at the bifurcation points of the diagram, it is enough to start the numerical procedure with a stable (unstable) limit cycle to calculate the whole stable (unstable) branch. Note also that, following the procedure reported in section 4.3, we have identified the cyclic fold bifurcations which define some of the intersections between stable and unstable branches.

- Neo-Hookean model: the $\lambda_{max} - \lambda_{min}$ excursions are tilted to the left. This behaviour is called softening and implies that in order to rise the amplitude of the oscillations a decrease in the applied frequency is required. Thereby, tilting of the resonance diagram makes that the nonlinear resonance frequency (maximum amplitude of the oscillation) occurs for $\bar{\omega} = 0.4$, away from the natural frequency of the aneurysm (onset of the main excursion) which is located at $\bar{\omega} \approx 1$. The amplitude of the nonlinear resonance frequency is ≈ 5.5. Besides the main resonance, we have identified six super-harmonics. The stable and unstable branches of each excursion are located on the right and on the left of the peak, respectively. Note that the maximum amplitude of the super-harmonics does not decrease monotonically as one moves away from the fundamental (primary) resonance of the aneurysm. The shorter excursion is the second super-harmonic starting from the fundamental resonance. This *unexpected* behaviour is most likely related to the fact that the peak of the excursions denotes the loss of the oscillatory behaviour of the shell. The aneurysm cannot sustain larger values of stretch within an oscillatory motion and expands unbounded (Rodríguez-Martínez et al., 2015; Aranda-Iglesias et al., 2015).

- Mooney-Rivlin model: the $\lambda_{max} - \lambda_{min}$ excursions are tilted to the right. This behaviour, called hardening, is different to the response provided by the Neo-Hookean model. Only the *foot* of the shortest super-harmonics is transiently tilted to the left, showing the so-called

snap-through behaviour. In general terms, the Mooney-Rivlin material requires an increase in the applied frequency to rise the amplitude of the oscillations. The nonlinear resonance frequency occurs for $\bar{\omega} = 34$, a value significantly greater than the natural frequency of the aneurysm. The amplitude of the nonlinear resonance frequency (≈ 2.6) is significantly smaller than in the case of the Neo-Hookean model. Moreover, we have identified six super-harmonic resonances. In contrast to the case of the Neo-Hookean model, the maximum amplitude of the super-harmonics decreases monotonically as one moves away from the fundamental resonance of the aneurysm. This is because now the maximum amplitude of the oscillations is not limited by loss of the oscillatory response of the aneurysm but by the external work applied to the system. The aneurysm could sustain larger values of stretch provided that a larger amount of external work is applied to the system (Rodríguez-Martínez et al., 2015; Aranda-Iglesias et al., 2015)

It becomes apparent the key role played by the constitutive model in the resonance diagram of the aneurysm. The strain energy function determines the amplitude of the oscillations and the nature (softening or hardening) of the interplay between the amplitude of the oscillations and the applied frequency.

On the other hand, it is critical to note that, taking into account the material and geometric parameters given in section 2, the values of $\bar{\omega}$ corresponding to the typical physiologic conditions of an aneurysm range between $2 \cdot 10^{-3}$ and $6.5 \cdot 10^{-3}$. This range is calculated assuming that the minimum and maximum heart rates are 60 and 190 beats per minute, respectively. According to Fig. 4, the aneurysm do not show resonances within these values of $\bar{\omega}$, i.e. our results suggest that the pulsatile blood flow cannot lead to the resonance of the aneurysm. This result agrees with the conclusions of Shah and Humphrey (1999) and David and Humphrey (2003) who already stated that the hypothesis of Simkins and Stehbens (1973) and Hung and Botwin (1975), who suggested that saccular aneurysms may be excited at their natural frequency by the pulsatile blood flow, may not be correct. Even in the case of the Neo-Hookean model for which the softening response brings the super-harmonics closer to the maximum frequency of the heart, there is a meaningful gap between the resonance frequency of the lowest super-harmonic $\left(1.5 \cdot 10^{-2}\right)$ and the frequency of the highest heart rate $\left(6.5 \cdot 10^{-3}\right)$.

Next, we further investigate the possibility of resonances in the aneurysm due to the pulsatile blood flow and, thanks to the 3D formulation derived in section 2, assess the effect of the wall thickness in the oscillatory response of the aneurysm.
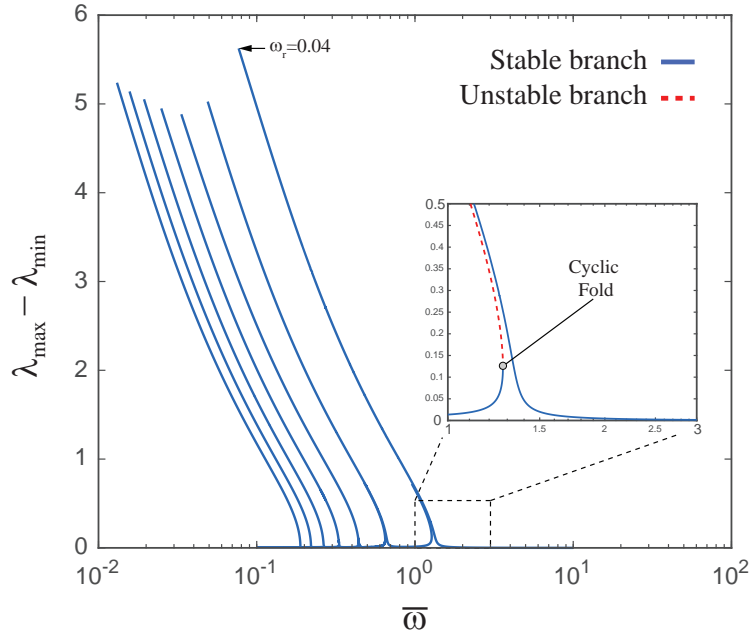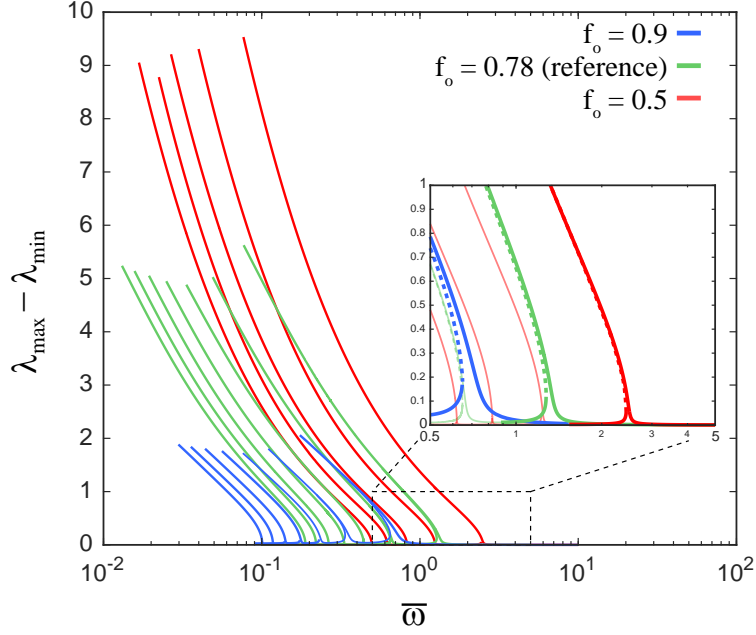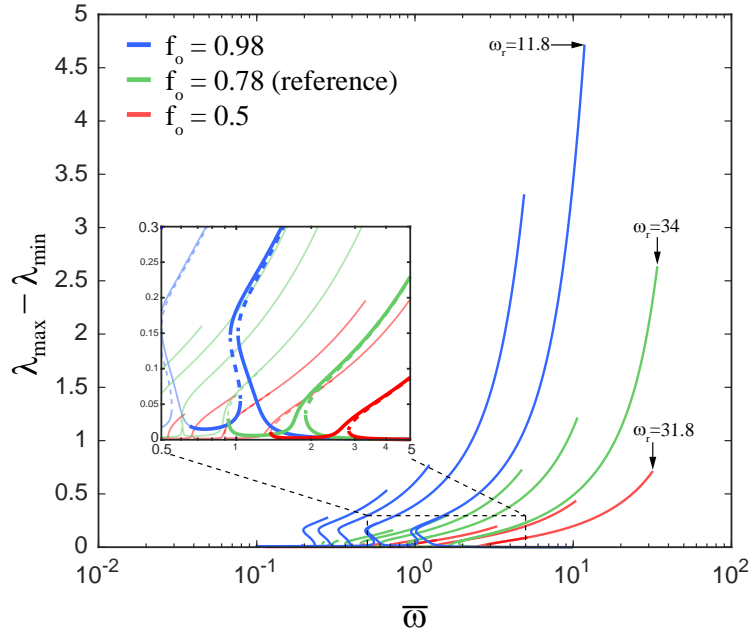
(a)
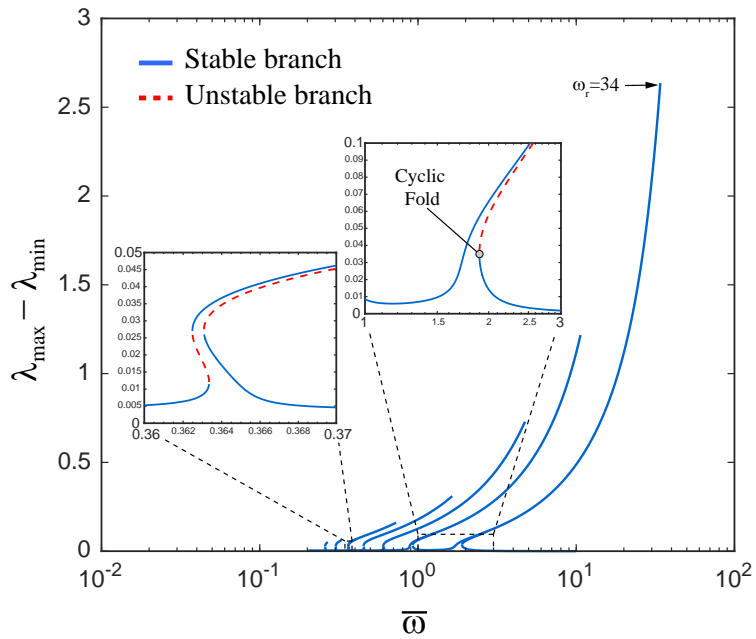
(b)

Figure 4: Resonance diagrams, $\lambda_{max} - \lambda_{min}$ versus $\bar{\omega}$, for (a) Neo-Hookean and (b) Mooney-Rivlin constitutive models. The reference geometric, loading and material parameters reported in sections 2 and 3 are used. The aneurysm is initially unstretched and at rest.

Fig. 5(a)-(b) shows the resonance diagrams, $\lambda_{max} - \lambda_{min}$ versus $\bar{\omega}$, for Neo-Hookean and Mooney-Rivlin constitutive models, respectively. Three different values of the thickness parameter f_0 are investigated: 0.9, 0.78 (reference) and 0.5 for the Neo-Hookean model and 0.98, 0.78 (reference) and 0.5 for the Mooney-Rivlin. The loading and material parameters reported in sections 2 and 3 are used. The following key observations arise from these graphs.

- The influence of f_0 in the amplitude of the oscillations of the aneurysm depends on the constitutive model. In the case of the Neo-Hookean model an increase of f_0 (smaller thickness) decreases the maximum amplitude of the resonances. As the thickness of the aneurysm decreases the oscillatory response of the shell is lost (the unbounded expansion of the shell starts) for smaller values of the ratio $\lambda_{max} - \lambda_{min}$. In fact, for $f_0 = 0.98$ (value investigated in the Mooney-Rivlin case) the aneurysm does not oscillate under this loading conditions. On the contrary, in the case of the Mooney-Rivlin model an increase of f_0 increases the maximum amplitude of the resonances. In this case the response of the aneurysm is oscillatory no matter the wall thickness and thus, as expected, the oscillations show larger amplitude as the thickness decreases.

- Irrespective of the constitutive model considered, the increase of f_0 (smaller thickness) shifts to smaller values of $\bar{\omega}$ the fundamental and the super-harmonic resonances of the aneurysm. The thinner the wall of the aneurysm, the closer are the resonance frequencies to the heart rate. Nevertheless, even in the case of the Neo-Hookean model, the lowest super-harmonic corresponding to the smallest thickness considered yet is far from the highest frequency of the pulsatile blood pressure. Thus, our results broaden the conclusions of Shah and Humphrey (1999) and David and Humphrey (2003) for a wide range of wall thicknesses and show that it is unlikely that resonances could lead to the enlargement and rupture of saccular aneurysms.

(a)

(b)

Figure 5: Resonance diagrams, $\lambda_{max} - \lambda_{min}$ versus $\bar{\omega}$, for (a) Neo-Hookean and (b) Mooney-Rivlin constitutive models. Three different values of the thickness parameter f_0 are investigated: 0.9, 0.78 (reference) and 0.5 for the Neo-Hookean model and 0.98, 0.78 (reference) and 0.5 for the Mooney-Rivlin.. The loading and material parameters reported in sections 2 and 3 are used. The aneurysm is initially unstretched and at rest. The reader is referred to the on-line version of the paper to distinguish the colour coding of the graphs in which the excursions corresponding to the smaller, intermediate and greater value of f_0 are red, green and blue, respectively.

6. Summary and conclusions

In this paper we have extended to a 3D framework the formulation developed by Shah and Humphrey (1999) to model the dynamic behaviour of idealized intracranial saccular aneurysms subjected to pulsatile blood flow and surrounded by cerebral spinal fluid. The need for a 3D formulation arises from the experimental measurements of Suzuki and Ohara (1978), MacDonald et al. (2000) and Costalat et al. (2011) who provided evidences of saccular aneurysms with ratios between wall thickness and inner radius larger that 0.1.

For the first time in literature, the dynamic response of the aneurysm has been analysed using nonlinear resonance diagrams obtained from a numerical procedure specifically designed for that purpose. Two different constitutive models have been used in the analysis: Neo-Hookean and Mooney-Rivlin. For each material model we have identified the fundamental resonance and six super-harmonics. A critical outcome of this research is to show that none of these resonances, for any of the constitutive models used and irrespective of the thickness of the aneurysm, lies within the frequencies associated to the normal heart rates. Thus, in agreement with David and Humphrey (2003), our results seem to discard the hypothesis of saccular aneurysms being led to rupture because they are excited at their natural frequency by the pulsatile blood flow. However, our results also show that the nonlinearities of the problem could bring closer than expected the resonance frequencies of the aneurysm to the usual frequencies of the heart. This finding, that has been rarely discussed in the literature, has been found strongly dependent on the constitutive model. It is thus highlighted that the description of the mechanical response of the aneurysmal wall has great influence on the dynamic response of these type of lesions.

References

Akkas, N., 1990. Aneurysms as a biomechanical instability problem. In: Biomechanical Transport Processes. Springer, pp. 303–311.

Allgower, E. L., Kurt, G., 1990. Numerical continuation methods: An introduction. Springer Series in Computational Mathematics.

Aranda-Iglesias, D., Vadillo, G., Rodríguez-Martínez, J. A., 2015. Constitutive sensitivity of the oscillatory behaviour of hyperelastic cylindrical shells. Journal of Sound and Vibration 358, 199–216.

Austin, G. M., Schievink, W., Williams, R., 1989. Controlled pressure-volume factors in the enlargement of intracranial aneurysms. Neurosurgery 24 (5), 722–730.

Costalat, V., Sanchez, M., Ambard, D., Thines, L., Lonjon, N., Nicoud, F., Brunel, H., Lejeune, J., Dufour, H., Bouillot, P., et al., 2011. Biomechanical wall properties of human intracranial aneurysms resected following surgical clipping (irras project). Journal of Biomechanics 44 (15), 2685–2691.

David, G., Humphrey, J. D., 2003. Further evidence for the dynamic stability of intracranial saccular aneurysms. Journal of Biomechanics 36 (8), 1143–1150.

Ferguson, G. G., 1972. Direct measurement of mean and pulsatile blood pressure at operation in human intracranial saccular aneurysms. Journal of Neurosurgery 36 (5), 560–563.

Gundiah, J., Ratcliffe, M. B., L., P., 2007. Determination of strain energy function for arterial elastin: Experiments using histology and mechanical tests. Journal of Biomechanics 40, 586–594.

Haslach, H. W., Humphrey, J. D., 2004. Dynamics of biological soft tissue and rubber: internally pressurized spherical membranes surrounded by a fluid. International Journal of Non-Linear Mechanics 39 (3), 399–420.

Humphrey, J. D., Haslach, H. W., 2003. Elastodynamics of saccular aneurysms: solid-fluid interactions and constitutive relations. Wall/Fluid Interactions in Physiologic Flows. WIT Press, Southampton.

Hung, E. J., Botwin, M. R., 1975. Mechanics of rupture of cerebral saccular aneurysms. Journal of Biomechanics 8 (6), 385–392.

Jain, J., 1963. Mechanism of rupture in intracranial saccular aneurysms. Surgery 54, 347–350.

Knowles, J. K., 1962. On a class of oscillations in the finite deformation theory of elasticity. Journal of Applied Mechanics 29, 283–286.

MacDonald, D. J., Finaly, H. M., B, C. P., 2000. Directional wall strength in saccular brain aneurysms from a polarized light microscopy. Annals of Biomedical Engineering 28, 533–542.

Ogden, R. W., 1997. Non-linear Elastic Deformations. Dover Civil and Mechanical Engineering. Dover Publications.

Peeters, M., Viguié, R., Sérandour, G., Kerschen, G., Golinval, J.-C., 2009. Nonlinear normal modes, part ii: Toward a practical computation using numerical continuation techniques. Mechanical Systems and Signal Processing 23 (1), 195 – 216, special Issue: Non-linear Structural Dynamics.

Rodríguez-Martínez, J. A., Fernández-Sáez, J., Zaera, R., 2015. The role of constitutive relation in the stability of hyper-elastic spherical membranes subjected to dynamic inflation. International Journal of Engineering Science 93, 31–45.

Ryan, J. M., Humphrey, J. D., 1999. Finite element based predictions of preferred material symmetries in saccular aneurysms. Annals of Biomedical Engineering 27, 641–647.

Sekhar, L., Heros, R., 1981. Origin, growth and rupture of saccular aneurysms: a review. Neurosurgery 8, 248–260.

Sekhart, L., Sclabassi, R., Sun, M., Blue, H., Wasserman, J., 1988. Intra-aneurysmal pressure mmeasurement in experimental saccular aneurysms in dogs. Stroke 19, 352–356.

Seydel, R. U., 1994. Practical Bifurcation and Stability Analysis: From Equilibrium to Chaos. SSpringer-Verlag.

Shah, A. D., Humphrey, J. D., 1999. Finite strain elastodynamics of intracranial saccular aneurysms. Journal of Biomechanics 32 (6), 593–599.

Simkins, T., Stehbens, W., 1973. Vibrational behavior of arterial aneurysms. Letters in Applied and Engineering Sciences 1 (85), 100.

Sracic, M. W., Allen, M. S., 2011. Numerical Continuation of Periodic Orbits for Harmonically Forced Nonlinear Systems. Springer New York, New York, NY, pp. 51–69.

Suzuki, J., Ohara, H., 1978. Clinicopathological study of cerebral aneurysms. Journal of Neurosurgery 48, 505–514.

Tóth, B., Raffai, G., Bojtár, I., 2005. Analysis of the mechanical properties of human brain aneurysm. Acta of Bioengineering and Biomechanics 7, 3–22.